

# 21 CM HYDROGEN-LINE SURVEY OF THE LARGE MAGELLANIC CLOUD

## II. DISTRIBUTION AND MOTIONS OF NEUTRAL HYDROGEN

By R. X. MCGEE\* and JANICE A. MILTON\*

[*Manuscript received November 16, 1965*]

### *Summary*

The 21 cm hydrogen-line data from a survey of the Large Magellanic Cloud with a  $14' \cdot 5$  aerial beam have been simplified into distributions of intensities and radial velocities at profile peaks. Fifty-two large HI complexes of mean diameter 575 pc, density 1 hydrogen atom per  $\text{cm}^3$ , and mass  $4 \times 10^6 M_\odot$  have been delineated. The study of the correlation between optically visible Population I components, such as HII regions and supergiant OB stars, and the neutral hydrogen has been greatly extended.

An analysis of the rotation of the galaxy, combined with the general velocity distribution and dispositions of the Population I components, has led to the proposal of a spiral arm structure for the Large Magellanic Cloud. The model consists of a principal plane containing two very large spiral arms and another plane, inclined to it at about  $20^\circ$ , containing two shorter arms emanating from each end of the stellar Bar. The total mass is estimated from the rotation and random-motions data at a lower limit of  $6 \times 10^9 M_\odot$ . The ratio of the mass of neutral hydrogen to the total mass is calculated to be in the range 5–9%.

### I. INTRODUCTION

Our knowledge of the Large Magellanic Cloud (LMC) up to 1963 has been summarized by two recent publications. Thackeray (1963) has reviewed all earlier published work, while contributors to the IAU-URSI Symposium No. 20 (Kerr and Rodgers 1964) have discussed more recent discoveries. Briefly, the LMC was seen to be an irregular galaxy exhibiting some possibility of spiral structure. Observational evidence indicated that it was rather flat, inclined to our line of sight, and rotating about an axis slightly removed from the centre of its most prominent optical feature, the great bar of stars.

We have investigated the neutral hydrogen content of the LMC with the advantage of much higher angular resolution than had been available previously. Some 5000 H-line profiles have been observed with the CSIRO 210 ft radio telescope, in several periods extending over  $2\frac{1}{2}$  years. The beamwidth was  $14' \cdot 5$ . A 48 channel line receiver was used with a coverage in radial velocity of 300 km/sec and spectral resolution of 7 km/sec.

In the present paper, we condense the original data to show the gas distribution in the form of contours of intensities and radial velocities at the H-line profile peaks. From such diagrams we are able to distinguish a number of enormous HI concentrations and to reinforce the previous findings (McGee 1964*a*—Paper I of the present series) on the association of the neutral hydrogen with other Population I components.

\* Division of Radiophysics, CSIRO, University Grounds, Chippendale, N.S.W.

The rotation of the Cloud is discussed and estimates of mass attempted. Finally, the accumulation of evidence shows the existence of well-defined spiral structure.

## II. EQUIPMENT AND OBSERVATIONAL METHOD

### (a) *Radio Telescope*

In H-line observations, the 210 ft paraboloid is fed by a circular waveguide horn whose aperture is flush with the metallic focal plane of approximately 10 wavelengths diameter. The primary radiation pattern slightly underfeeds the paraboloid, and the resulting beam is approximately circular with a width between half-power points of  $14' \cdot 5$  arc. Side lobes were found by observation of strong radio sources to be below 1%. An efficiency factor, defined as the ratio of radiation received from sky alone to the radiation from sky and ground contribution in the spillover, has been measured in several experiments at 0.8. The telescope pointing accuracy is better than  $1'$  arc.

### (b) *Receiver*

A description of the multichannel line receiver together with the procedures of setting up, operating, and calibrating have been given by McGee and Murray (1963). In the present observations, the 48 channels were 37 kc/s or 7.8 km/sec wide at the half-power points and were spaced at 33.2 kc/s or 7.0 km/sec across the reception band. The time constant used was 65 sec.

The sensitivity of all channels could be checked at any time by the use of radiation from a noise lamp modulated at the same switching frequency as applied to the local oscillators.

### (c) *Intensity Calibration*

The temperature scale at the receiver output was established by the use of a number of accurately calibrated attenuators and directional couplers placed between an argon discharge lamp and the noise insertion point in the primary horn. One division of intensity in the arbitrary scale used in the diagrams of the present paper is equivalent to  $1.4$  degK of aerial temperature. This result depends on an assumption that the temperature of the commercial discharge lamp remained at the rated  $10100^\circ\text{K}$  and that all the equivalent power was coupled into the testing circuit. (A performance test was made at the National Standards Laboratory, CSIRO, before the lamp was put into operation.) An error of  $\pm 10\%$  is estimated for the measurement.

This calibration was consistent with observations of a number of discrete sources of known intensity and estimates of the sensitivity made from direct measurement of the receiver noise figure and output noise fluctuations.

### (d) *Observational Method*

Previous observations had suggested that the approximate limits of the neutral gas in the LMC were  $04^{\text{h}} 30^{\text{m}}$  and  $06^{\text{h}} 20^{\text{m}}$  in right ascension and  $-64^\circ$  and  $-78^\circ$  in declination. The survey was carried out over this area, with some additional observations outside it at points where gas was suspected to exist. The method

was to track the telescope along lines of constant declination at a rate of 3' arc per minute of time. Since one profile was recorded every 2 min, the rate ensured that more than two complete profiles were observed per aerial beamwidth. The spacing in declination was 12' arc over most of the Cloud, and 6' in the complex region bounded by right ascension lines  $05^{\text{h}}30^{\text{m}}$  and  $06^{\text{h}}00^{\text{m}}$  and declination lines  $-68^{\circ}30'$  and  $-71^{\circ}30'$ . A number of tracks at constant right ascension at 3' arc per minute in declination were made. From these and some stationary observations at high intensity points, the effects of blurring due to the movement of the telescope and the receiver time constant could be ascertained. Ninety close coincidences of position from both right ascension and declination tracks were available for direct comparisons; approximately 20% of these show differences of up to 10% in peak intensities. In most cases, the radial velocities of profile peaks agreed within the expected accuracies, i.e.  $\pm 2$  km/sec. Calibration for the receiver baseline, which showed slow changes presumed to be due to changing temperature at the front end of the receiver, were made between each track, i.e. at intervals of about 3 hr. They were recorded at positions of zero hydrogen as close as practicable to the beginning or end of a track. Sensitivity calibrations were made at the beginning and end of each observing session.

The H-line profiles were recorded both on a pen recorder and on punched paper tape. The latter was processed in an electronic computer in the same general way as reported by Hindman *et al.* (1963).

The positional information from the telescope control desk, also recorded on punched paper tape every 2 min, and a continuous log of operating frequencies measured with a frequency counter, were combined in the computer to provide radial velocities corrected to the Sun for each H-line profile.

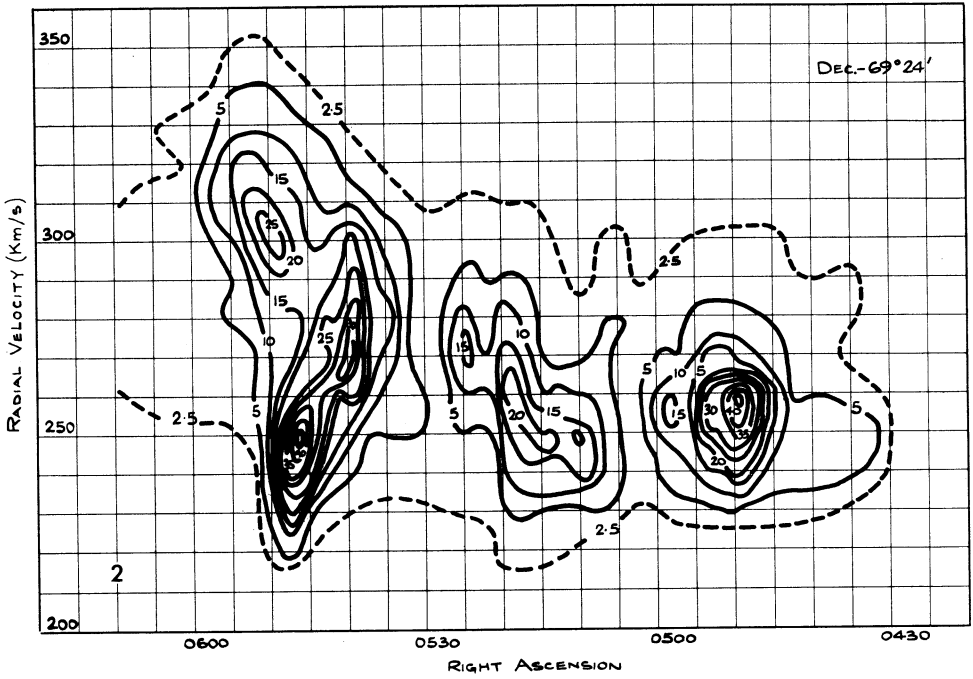
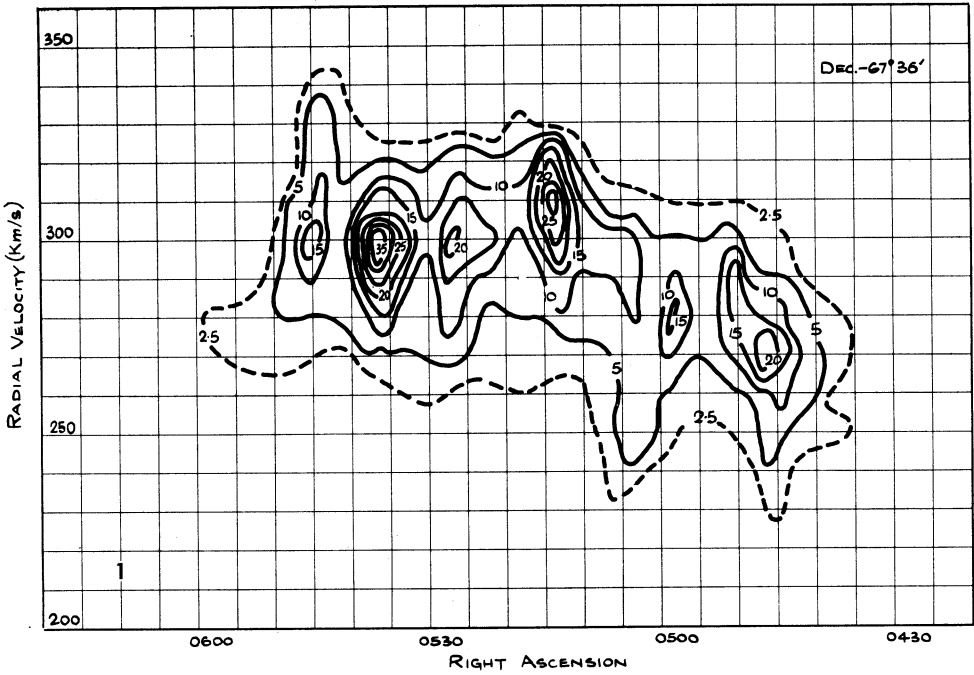
### III. BASIC DATA

Although the entire observational data have been reduced to 70 diagrams, they are still too numerous for presentation here and appear in a supplement to this Journal as Paper III of the present series (McGee and Milton 1966). Sixty-seven of the diagrams are in the form of relative intensity contours plotted on coordinates of radial velocity and right ascension for constant declinations across the LMC; the remaining three are on coordinates of radial velocity and declination for constant right ascensions. Three samples are given in Figures 1, 2, and 3 of the present paper.

The contours are spaced at intervals of 5 arbitrary or "computer" units (7 degK in aerial temperature  $T_a$  or 8.8 degK in brightness temperature  $T_b$ ) and drawn through points approximately  $1^{\text{m}}$  apart in right ascension and 10 km/sec apart in radial velocity. The information has been taken directly from the observed H-line profiles, and no smoothing of contours has been introduced.

The diagrams are useful for condensing the data, and H-line profiles for individual positions can easily be reconstructed from them. However, they are not well suited for giving the overall picture of the HI distribution.

The sample diagrams (Figs. 1, 2, and 3) illustrate the trend of all the results, which show large complexes of HI embedded in a fairly low-level background.



Figs. 1 and 2

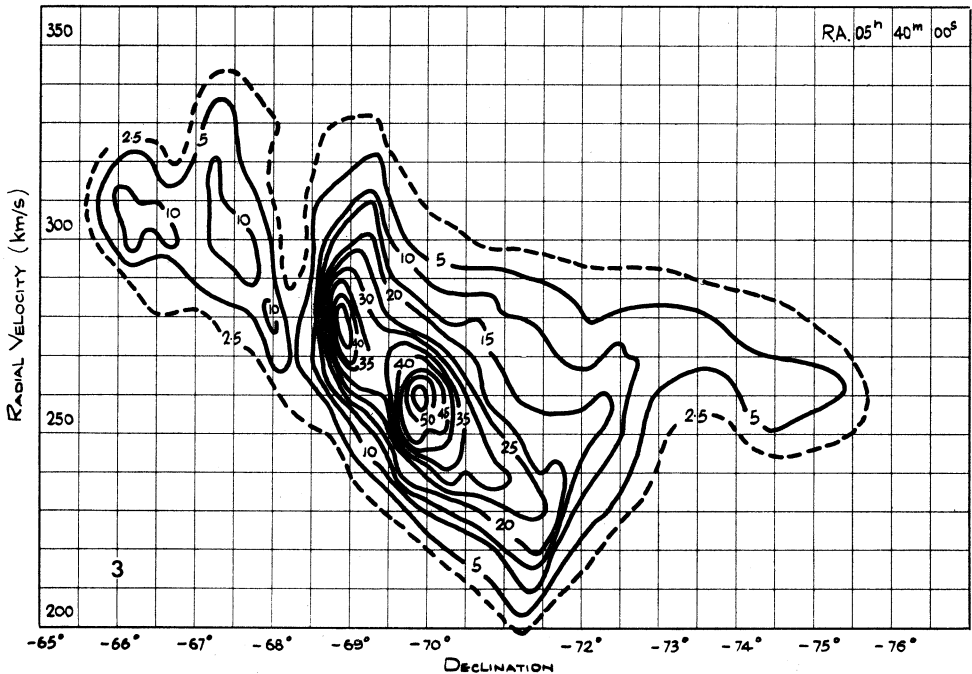


Fig. 3.—Contours of relative intensity of 21 cm H-line radiation. Coordinates are radial velocity and declination. The contour interval is 5 units (1 unit = 1.4 degK of  $T_a$ ).

The maxima of the complexes seem to occur at velocities within  $\pm 10$  km/sec of +240, +270, and +300 km/sec. The previously observed general gradient in radial velocity from south to north across the galaxy is clearly seen in Figure 3.

A preliminary impression of the velocity distribution may be gained from Figure 4. The coordinate grid encloses areas  $1^\circ$  in declination by  $10^m$  in right ascension, and listed in each area are the average radial velocities at the H-line profile peaks. In some areas only one peak was present in the profiles, in most two peaks were present, and in about 10% of profiles three peaks were observed. The numbers in Figure 4 represent averages of from 20 profiles (in fringe areas) to 80 (in more complicated regions).

It appears that three distinct ranges of radial velocity exist. In northern declinations only the two higher are present, in southern declinations the two lower, and at regions near  $05^h 05^m$ ,  $-68^\circ$ , and  $05^h 50^m$ ,  $-70^\circ$ , all three are present. The means of these representative velocities are +300, +273, and +243 km/sec, with standard deviations less than  $\pm 8$  km/sec.

Having recognized the presence of these velocity groups, we proceed to a further simplification of the data by presenting contours of the peak H-line intensities

Figs. 1 and 2 (*opposite page*).—Contours of relative intensity of 21 cm H-line radiation. Coordinates are radial velocity and right ascension. The contour interval is 5 "computer" units (1 unit = 1.4 degK of  $T_a$  = 1.75 degK of  $T_b$ ).

$T_{\max}$  (McGee, Murray, and Milton 1963) for each of the three groups. A composite map is given in Figure 5, where three colours have been used to distinguish the different contributions. Blue indicates gas at velocities around +243 km/sec, orange near +273 km/sec, and red near +300 km/sec. Deeper shades denote increased intensities. The fine outer contours represent the limit at which the hydrogen can

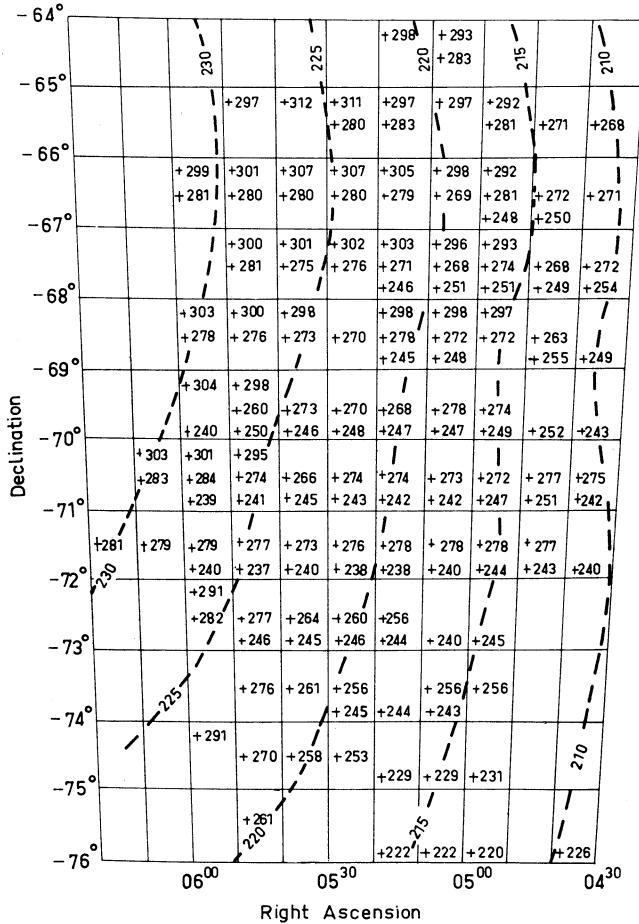


Fig. 4.—Averages of radial velocities at H-line peaks over areas  $1^\circ$  in declination by  $10^m$  in right ascension. Values are referred to the Sun. The contours give the corrections that must be subtracted from the observed velocities to allow for the rotation  $\theta_0 = 250$  km/sec at the Sun.

be detected with the present equipment. The HI, then, is contained within the approximate limits in right ascension of  $04^h 30^m$  and  $06^h 00^m$ , with a narrow extension to  $06^h 20^m$  near declination  $-71^\circ$ , and within the limits in declination of  $-64^\circ 30'$  and  $-76^\circ$  approximately. Most of the gas lies within a radius of  $4\frac{1}{2}^\circ$  of a central position. The gas south of declination  $-73^\circ$  is of very low intensity. The present



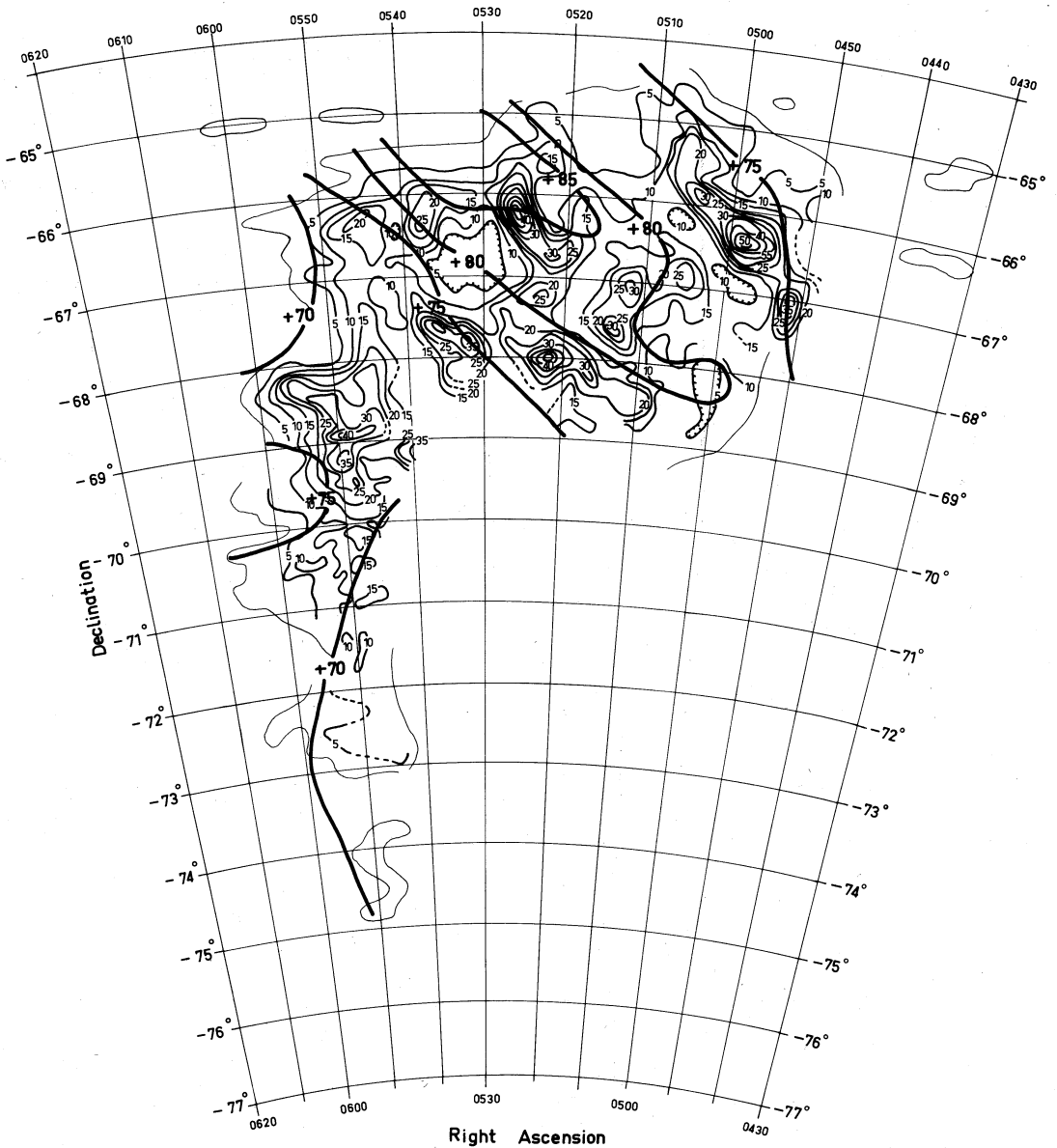


Fig. 6(a).—Contours of H-line peak intensities  $T_{\max}$  over the Large Magellanic Cloud for gas at radial velocities near +300 km/sec. The contour interval is 5 units (1 unit = 1.4 degK of  $T_{\Delta}$ ). Contours of radial velocity (interval 5 km/sec) are superimposed in red (values corrected for  $\theta_0 = 250$  km/sec).

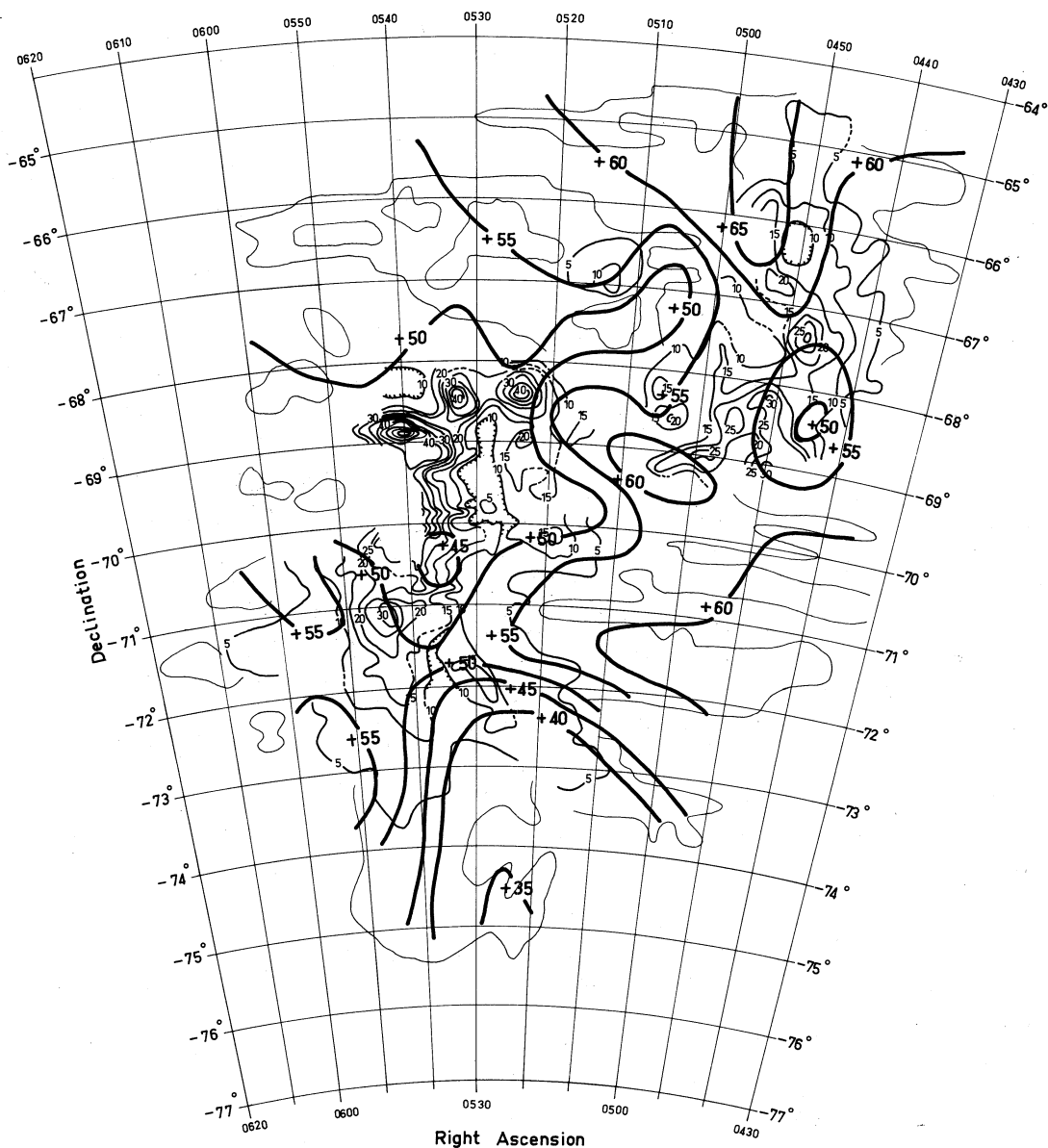


Fig. 6(b).—Contours of H-line peak intensities  $T_{\max}$  over the Large Magellanic Cloud for gas at radial velocities near  $+273$  km/sec. The contour interval is 5 units (1 unit =  $1.4$  degK of  $T_a$ ). Contours of radial velocity (interval 5 km/sec) are superimposed in red (values corrected for  $\theta_0 = 250$  km/sec).

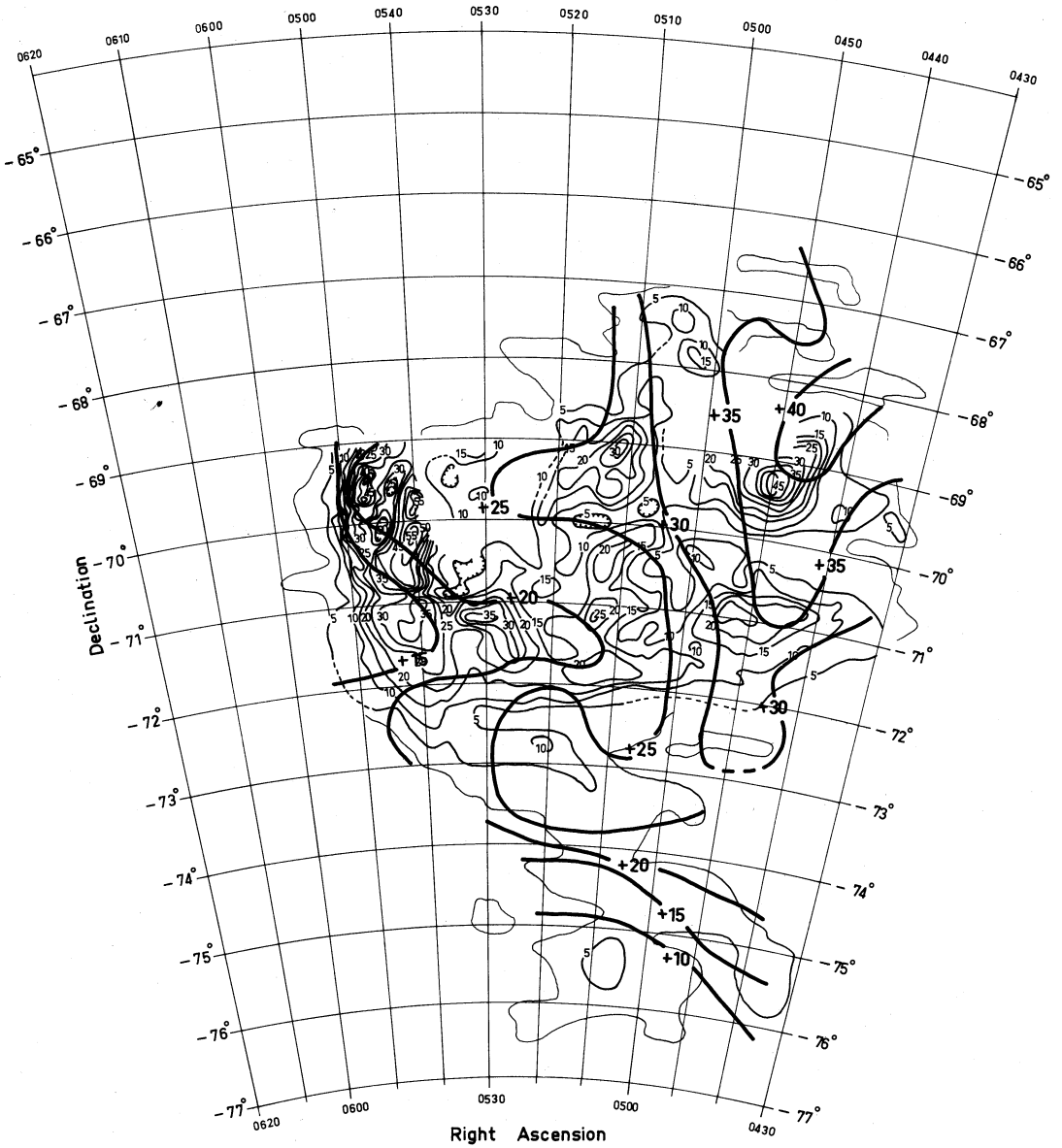


Fig. 6(c).—Contours of H-line peak intensities  $T_{\max}$  over the Large Magellanic Cloud for gas at radial velocities near +243 km/sec. The contour interval is 5 units (1 unit = 1.4 degK of  $T_a$ ). Contours of radial velocity (interval 5 km/sec) are superimposed in red (values corrected for  $\theta_0 = 250$  km/sec).

limit is at least  $1\frac{1}{2}^\circ$  less than the radius obtained by Hindman, Kerr, and McGee (1963) with a much wider aerial beam.

Brief observations were made in the "bridge" region between the Large Magellanic Cloud and the Small Magellanic Cloud, but only isolated patches of gas were detected at the low level.

A detailed contour map of intensities  $T_{\max}$  for each radial velocity range is given in Figures 6(a), 6(b), and 6(c). Contours of radial velocity at  $T_{\max}$  are superimposed in red. The latter have been greatly smoothed by being drawn through mean values per unit area ( $1^\circ$  in declination by  $10^m$  in right ascension). The velocities are adjusted for a galactic rotation at the Sun of 250 km/sec. It may be noted that the intensity distribution in two of the diagrams ((a) and (b)) strongly resembles those observed in the spiral arms of our Galaxy (McGee and Milton 1964).

#### IV. THE LARGE COMPLEXES OF NEUTRAL HYDROGEN IN THE LMC

The outstanding features of Figures 6(a)–6(c) are the concentrations of closed contours, indicating that rather large complexes of neutral hydrogen are the main constituents in each velocity range.

Some of the physical properties of the complexes have been investigated and are set out in Table 1 together with information on associated optical objects. Catalogue numbers have been given to those bodies of gas delineated by closed contours. Additional features such as spurs of HI have been included unnumbered where there is obvious correlation with important visible objects.

The coordinates of right ascension and declination are those at the intensity maxima of the complexes. Columns 4 and 6 of Table 1 contain the values of radial velocity, referred to the Sun, and of maximum H-line brightness temperature. The dispersions  $\sigma$  derived from the average half-widths of all the profiles associated with a complex are given in column 5. Correction for instrumental smoothing has been applied; the corrections were 10% for the narrowest lines and approximately 4% on average.

The values given in columns 7–9 are "estimated quantities", since a number of assumptions are required in deriving them, as explained in 1 and 2 below.

##### 1. *Diameters*

The diameters measured in the right ascension and declination directions are quoted in parsecs and are based on a value of 52 kpc for the distance of the LMC. This is a compromise between recent evaluations of 50 and 55 kpc by Gascoigne and Kron (1965) and Thackeray (1963) respectively.

##### 2. *Average Density $\bar{n}_H$ and Mass*

The first requirement in the calculation of gas density is an estimate of the optical depth. We may write for optical depth (Wild 1952):

$$\tau(\nu) = \frac{3A_{21}c^3h}{32\pi\nu^2k} \cdot \frac{1}{T_e} f(V) \int_0^\infty n_H ds, \quad (1)$$

TABLE I  
 PHYSICAL PROPERTIES OF NEUTRAL HYDROGEN COMPLEXES AND ASSOCIATED OPTICAL OBJECTS IN THE LARGE MAGELLANIC CLOUD

HI Concentration No.	Position (1964)		Radial Velocity* (km/sec)	Dispersion (km/sec)	$T_b$ (°K)	Diameters† (pc)	$\bar{n}_H^\ddagger$ (atoms/cm <sup>3</sup> )	Mass‡ (10 <sup>6</sup> M <sub>⊙</sub> )	HII Regions near HI Concentrations	Supergiant Stars with Similar Radial Velocities	Relative Intensity of 21 cm Continuum	Notes
	R.A. h m	Dec. °										
L1	04 51.5	-67 05	+294	11.9	63	360 670	1.7	2.9	N 4(+292), N 5, N 9	R 51(+306), R 53(+309), R 56(+312), R 57(+301), R 61(+286), R 62(+295)	5	The radio continuum and HI contours have the same general structure over these three concentrations and a north-going spur near 05 <sup>h</sup> 06 <sup>m</sup> , -65°15'
L2	04 58.3	-66 23	+294	12.3	89	650 550	1.7	6.6	N 11(+296, +303, +202), N 12, N 13, N 14	R 68(+313), R 70(+300)	23	
L3	05 04.1	-65 54	+301	10.1	53	510 380	1.2	1.7	—	—	4	
L4	05 05.1	-66 53	+298	11.0	47	580 700	0.7	3.2	N 17(+289)	R 73(+305), R 74(+299), R 75(+297)	5	
—	05 10	-68 33	+293	12	44				N 104			HI spur; not listed as an individual concentration
L5	05 11.9	-67 04	+300	9.6	53	600 810	0.7	4.0	—	—	—	A continuum source of rel.int. 10 units is situated approximately midway between L5 and L6 Stars away from HI at +300 km/sec
L6	05 13.6	-67 35	+307	12.8	54	550 440	1.3	2.7	N 30	R 79(+302), R 85(+292), R 87(+286), R 88(+295), R 89(+285), R 103(+298)	—	
L7	05 16.6	-68 10	+298	11.9	53	410 570	1.3	2.5	—	—	—	HI spur
—	05 18	-66 04	+312	14	24				N 35			
L8	05 21.8	-66 47	+308	10.1	53	550 460	1.0	2.3	N 37	—	5	The young association NGC 1929-37 corresponds in position (Bok 1964)
L9	05 21.8	-68 00	+298	10.5	81	650 570	1.3	5.5	N 44(+296, +296)		21	
L10	05 22.7	-65 37	+308	7.3	33	360 360	0.5	0.5	N 43	R 92(+322), R 94(+291), R 95(+329), R 97(+308), R 98(+308)	4	
L11	05 23.0	-67 13	+306	11.9	47	580 460	1.0	2.4	N 50		—	HI spur between L9, L11, and L13 Weak HI feature
L12	05 26.2	-66 14	+308	11.4	82	350 650	2.3	3.7	N 48	R 104(+306)	15	
—	05 27	-67 40	+300	17	35				N 51	R 108(+311)	11	
—	05 32	-66 28	+307	8	18				N 55(+302)			
L13	05 32.2	-67 49	+298	9.2	66	450 520	1.1	2.3	N 57(+306)	R 107(+336), R 117(+317), R 118(+342), R 119(+312)	11	Stars in weak HI region
—										R 120(+288), R 121(+319), R 125(+292)		
L14	05 36.0	-67 37	+298	10.1	63	380 420	1.4	1.6	N 56, N 59		16	

L15	05 37.8	-66 22	+307	9.6	46	380 520	0.9	1.4	N 62, N 63, N 64, N 65	10	Extension at lower level in continuum source corresponds to HI maximum
	05 44	-67 30	+300	11	28				N 70, N 74	3	HI spur
L16	05 45.7	-66 18	+304	8.7	39	650 670	0.4	2.2	N 72(+307)		III and radio source displaced from HI maximum
L17	05 48.2	-69 30	+298	13.2	53	700 580	1.0	4.6	N 169		
L18	05 49.4	-68 54	+304	14.1	74	550 700	1.6	6.7			
L19	05 49.6	-69 10	+306	16.7	65	600 760	1.6	8.6	N 75		
	05 56	-68 12	+300	11	47						
L20	04 47.3	-67 21	+272	9.6	53	580 800	0.7	3.7	N 3		
L21	04 50.8	-68 12	+270	8.7	53	870 490	0.8	3.3	N 8(+284), N 76		
L22	04 52.2	-66 46	+286	12.3	37	870 580	0.7	4.1			
L23	04 55.0	-68 31	+278	9.6	53	520 700	0.8	3.0	N 91(+278), N 84	5	III regions in an HI intensity dip between L23 and L24
									N 86, N 92		
L24	04 58.7	-68 59	+276	9.6	49	860 420	0.9	2.7		4	
L25	05 03.7	-68 34	+272	10.5	35	540 410	0.7	1.2			
L26	05 05.4	-68 13	+264	13.6	32	400 700	0.8	1.4	N 23	6	
L27	05 13.4	-66 54	+280	11.0	23	640 580	0.3	1.3			
L28	05 19.5	-70 09	+263	(20.6)	28	540 460	0.9	2.0			
L29	05 23.6	-69 00	+270	9.6	39	550 650	0.6	2.3			
L30	05 24.0	-68 23	+268	11.4	77	480 440	1.7	3.1	N 138(+276)	8	
	05 26	-69 18	+273	11	30				N 140, N 142, N 143	25	Weak HI feature
	05 27	-68 52	+270	14	25				N 144	10	At north end of a trough of HI
L31	05 32.5	-68 26	+277	13.2	72	480 600	1.6	4.4	N 148(+272)	12	
	05 34	-69 45	+270	17	31			1	N 149(+276), N 154(+268)	18	Complex region; no individual concentrations recognized
L32	05 40.1	-68 52	+276	15.8	112	810 550	2.8	13.6	N 164, N 165, N 157(+260), 30 Dor.	210	In addition to the dimensions given, the HI concentration has a large plateau at $T_b = 70^{\circ}\text{K}$
L33	05 43.5	-71 06	+277	14.5	58	800 830	0.8	8.4		7	
L34	04 50.2	-69 17	+257	9.2	82	760 640	1.0	6.1	N 77(+248), N 79(+246), N 83(+265, +254), N 81A, B; N 94	3 max 7, 9, 6	
L35	[04 50.2	-70 59	+250	10.1	47	890 580	0.8	4.5		6	
	[04 53.0	-70 58			53						
L36	04 58.6	-70 18	+245	8.7	18	670 450	0.3	0.8	N 185, N 186	5	
L37	05 02.5	-67 52	+257	10.1	28	460 440	0.5	0.9	N 16, N 16A		N 21 lies between L37 and L38
L38	05 04.6	-67 25	+252	10.1	23	610 360	0.5	0.8			
	05 05	-70 48	+248	20	19				N 190		Weak HI feature
	05 05	-70 58	+250	13	19				N 191A(+242)		Weak HI feature
									R 52(+262)		
									R 66(+271 $\sim 1^{\circ}$ away)		
									R 64(+275)		
									R 58(+271)		
									R 105(+268)		
									R 111(+260), R 123(+267), R 126(+258), R 127(+284), R 128(+268)		
									R 129(+273), R 131(+269), R 136(+274), R 143(+263)		
									R 54(+250), R 55(+268), R 59(+258), R 65(+258)		
									R 67(+244) R 76(+253)		
									R 71(+198), R 72(+237), R 80(+231)		

† Estimated quantities only.

\* Referred to the Sun.

TABLE 1 (Continued)

HI Concentration No.	Position (1964)		Radial Velocity* (km/sec)	Dispersion (km/sec)	$T_b$ (°K)	Diameter (pc) R.A. Dec.	$\bar{n}_{HI}^\dagger$ (atoms/cm <sup>2</sup> )	Mass† (10 <sup>6</sup> M <sub>⊙</sub> )	HII Regions near HI Concentrations	Supergiant Stars with Similar Radial Velocities	Relative Intensity of 21 cm Continuum	Notes
	R.A. h m	Dec. ° ' "										
L39	05 11.4	-69 04	+255	10.1	58	480 570	0.9	2.3	N 105(+256), N 103, N 100	R 78(+238), R 81(+227)	13	L37, L38, L39, L40, and L43 are components of a large north-going spur of HI, which starts at about 05 <sup>h</sup> 20 <sup>m</sup> , -70°30'. The narrow southern part of the spur corresponds in position to the well-known lane of obscuration across the optical Bar
L40	05 12.5	-69 33	+246	9.6	44	570 380	0.9	1.4	N 113(+233), N 114	R 82(+236), R 84(+262)	10	Weak HI spur between L42 and L46
L41	05 12.7	-70 31	+246	9.2	44	460 540	0.7	1.6	N 193(+247)	—	5	
L42	05 13.6	-71 09	+233	9.2	46	510 460	0.7	1.5	N 195	—	—	
L43	05 18.2	-71 17	+256	16.7	40	390 510	1.4	2.1	N 117(+269), N 119, N 120(+251, +257), N 121(+243), N 127(+259)	—	10	
L44	05 20.9	-72 45	+251	10.1	19	600 320	0.5	0.6	—	—	—	Weak HI Feature
L45	05 21.1	-70 49	+240	8.7	35	440 440	0.5	0.8	—	R 96(+241),	—	
L46	05 26.0	-71 35	+238	9.6	54	770 870	0.5	5.1	N 198, N 200, N 205	R 100(+251),	5	
L47	05 28 05 31.4	-70 36 -71 12	+246 +240	10 9.6	28 67	760 450	1.2	3.6	N 204 N 206(+240)	R 101(+251)	12	
L48	05 39.8 05 40.5	-69 43 -69 53	+255 +258	16.7	102 105	410 700	3.7	8.8	N 159(+252, +254), N 160(+246, 254), N 177, N 158	R 112(+237), R 113(+244), R 122(+257) R 150(+241), R 152(+258)	44	Star away from HI The peaks of the "+243" and "+273" contributions are hard to distinguish in this region; unfinished contours are given on the west side of these sources
L49	05 40.5	-70 10	+255	15.8	100	570 870	2.4	13.3	N 218(+239), N 219(+242), N 213(+236), N 175	—	9	Corresponds with extension of continuum contours in the 30 Dor. complex
L50	05 40.5	-71 03	+241	18.0	70	870 1090	1.2	19.6	N 214(+236)	—	7	L50 and L51 correspond in positions with extensions of continuum 30 Dor. complex
L51	05 46.6	-69 26	+246	11.9	88	450 490	2.0	3.7	—	R 133(+235),	—	16
L52	05 47.3	-69 43	+244	11.0	91	450 730	1.9	5.6	N 168(+243), N 163, N 180	R 153(+253), R 154(+242), R 155(+248)		

† Estimated quantities only.

\* Referred to the Sun.

where  $A_{21}$  is the transition probability for the line ( $= 2.85 \times 10^{-15} \text{ sec}^{-1}$ ), the fundamental constants  $c$ ,  $h$ , and  $k$  have their usual significance,  $V$  is the radial velocity,  $\nu$  is the frequency,  $T_e$  is the excitation temperature,  $n_H$  is the number density of hydrogen atoms per  $\text{cm}^3$ , and  $f(V)$  is the "line-shape" function.

Also, the number of hydrogen atoms per  $\text{cm}^2$  in a line-of-sight column is

$$N_H = \int_0^\infty n_H ds. \quad (2)$$

Thus,

$$\tau(\nu) = 5.45 \times 10^{-14} \frac{N_H}{T_e} f(V) = \tau(V). \quad (3)$$

To make an approximate estimate for  $f(V)$ , we have assumed that the line radiation from a gas complex produces a Gaussian-shaped profile which is then corrected for instrumental smoothing. The dispersion  $\sigma$  is (half-width)/2.35, and, writing  $V_p$  as the radial velocity at the profile peak, we have for the line-shape function

$$f(V) = \frac{1}{\sigma(2\pi)^{\frac{1}{2}}} \exp\{-\frac{1}{2}(V - V_p)^2/\sigma^2\}. \quad (4)$$

In earlier H-line work,  $125^\circ\text{K}$  was used for  $T_e$ , but recently higher values have been proposed (e.g.  $135^\circ\text{K}$  by Raimond (1966)). However, H-line temperatures of  $160^\circ\text{K}$  and more have been observed for emission profiles with the 210 ft telescope. After making a series of test calculations of optical depths in the LMC at various values of  $T_e$ , we conclude that  $200^\circ\text{K}$  gives more plausible values of  $\tau$ .

Following from equation (4), we obtain

$$\tau(V) = \tau(V_p) \exp\{-\frac{1}{2}(V - V_p)^2/\sigma^2\},$$

therefore,

$$\tau(V_p) = \frac{5.45 \times 10^{-14} N_H}{\sigma(2\pi)^{\frac{1}{2}} T_e}; \quad (5)$$

thus,

$$N_H = \sigma \tau(V_p) \times 0.92 \times 10^{21} \quad (6)$$

for  $T_e = 200^\circ\text{K}$  and with  $\sigma$  expressed in km/sec;  $\tau(V_p)$  is related to the observed  $T_{\text{max}}$  by

$$\tau(V_p) = -\ln(1 - T_{\text{max}}/T_e).$$

The information contained in the basic data (Paper III) shows that the gas in the LMC lies in the total velocity range of  $+190$  to  $+360$  km/sec and may be considered quite separate from other contributions (e.g. the galactic emission near  $0$  km/sec). Therefore, in equation (2),

$$\int_0^\infty ds = \int_{l_1}^{l_2} ds,$$

where  $l_1$ ,  $l_2$  represent the limits of the gas in the LMC in our line of sight. This idea may be further extended to the dimensions of a particular gas complex. The line-of-sight dimension of a complex needs to be assumed, and we have taken it as the mean of the right ascension and declination dimensions in estimating  $\int_{l_1}^{l_2} ds$ . The

average gas density  $\bar{n}_H$  is finally obtained from equation (2), and the mass estimate follows.

*Discussion of the Values Given in Table 1*

(i) *Radial velocities.*—The values of the radial velocities of the HI complexes occur in three definite groups: +293 to +312 km/sec, +263 to +286 km/sec, and +223 to +256 km/sec. The table is arranged so that three groups L1–L19, L20–L33, and L34–L52 respectively cover these velocity ranges.

(ii) *Dispersion.*—The dispersions vary between 7.3 and 20 km/sec, with a mean of 11.5 km/sec. This is exactly the same value as that found in the local galactic region with a  $2^\circ.2$  aerial beam (McGee, Milton, and Wolfe 1966). The central point of each complex has been subsequently observed with an additional system of narrow-band filters (15) of half-power width 2 km/sec spaced at intervals of 2.0 km/sec, but no evidence of the peaks splitting up into components was recognized.

TABLE 2

MEAN ESTIMATED PHYSICAL QUANTITIES IN THE HI COMPLEXES OF THE LARGE MAGELLANIC CLOUD

	Dimension (pc)		Dispersion (km/sec)	$N_H$ (max. value) (atoms/cm <sup>2</sup> )	$\bar{n}_H$ (atoms/cm <sup>3</sup> )	Complex Mass ( $10^6 M_\odot$ )
	R.A.	Dec.				
+300 range	520	570	11.1	$3.8 \times 10^{21}$	1.2	3.5
+273 range	650	580	12.0	$3.6 \times 10^{21}$	1.0	3.9
+243 range	580	570	11.4	$4.4 \times 10^{21}$	1.1	4.2
Whole Cloud	580	570	11.5	$4.0 \times 10^{21}$	1.1	3.9

(iii) *Brightness temperature.*—The values vary widely between 18 and 112°K.

(iv) *Estimated dimensions.*—The dimensions for single complexes have a relatively small range, 320 to 870 pc, with a mean diameter of 575 pc. Thus, they are similar in size to the largest class of HI clouds in our own Galaxy (McGee 1964*b*; McGee and Milton 1964).

(v) *Estimated density.*—The mean density in Table 1 is 1 hydrogen atom per cm<sup>3</sup>; the range is 0.3–3.7 hydrogen atoms per cm<sup>3</sup>. Again, close agreement with galactic HI clouds may be noted.

(vi) *Estimated mass.*—The average mass is  $4 \times 10^6 M_\odot$ .

Table 2 sums up the above quantities and shows that the averages are similar in each of the three velocity ranges. The estimated average values of  $N_H$  at the maxima of the complexes have been included.

V. RELATION BETWEEN NEUTRAL HYDROGEN AND  
THE POPULATION I AND II OBJECTS

(a) *Population I*

The remainder of Table 1 shows how the most prominent optically observed objects of Population I associate with the neutral gas. Column 10 is a list of 90 HII regions of size greater than  $2'$  by  $2'$  arc from the Henize (1956) catalogue. For 29 of

the nebulae, both the position and radial velocities measured by Feast (1964*a*) make close association with particular HI complexes certain. Forty-one others may be associated with complexes on positional evidence only. Twenty of the 90 are associated not with complexes but with comparatively minor HI features; their positions are recorded and comments made in column 13.

A similar procedure has been adopted with the supergiant stars (mostly of OB classification) for which radial velocities have been measured by Feast, Thackeray, and Wesselink (1960). The numbering system (R 51, etc.) is from the Radcliffe Observatory catalogue.

Some statistics concerning the high correlation between the motions of the HI, HII, and supergiant stars have been given in Paper I (McGee 1964*a*).

The radio continuum intensities (in arbitrary units) at 1410 Mc/s, taken from the diagram by Mathewson and Healey (1964), are included in column 12. The correspondence in radio continuum contours and HI contours is even more marked in the present peak-intensity diagrams than in the earlier integrated brightness diagram (Bok 1964).

The spatial correspondence of the Population I type component is strikingly emphasized in Figures 7(*a*), 7(*b*), and 7(*c*). Some of the gas  $T_{\max}$  contours have been redrawn to form a background. The positions of the maxima of the HI complexes are marked with a cross and labelled L1, L2, etc. The HII regions for which radial velocities are known are indicated by black circles. Open circles are at the approximate positions of other HII regions. Henize catalogue numbers N1, N2, etc. are included. The supergiant stars with Radcliffe catalogue numbers are shown by star signs.

Figure 7(*a*) contains all the known HII regions and supergiant stars whose velocities are near +300 km/sec. Similarly, Figure 7(*b*) has all those near +273 km/sec and Figure 7(*c*) all those near +243 km/sec.

Two interesting exceptions to the general Population I pattern have been pointed out by Westerlund (1964). The large hole in the "+300" HI distribution (Fig. 6(*a*)) at  $05^{\text{h}} 32^{\text{m}}$ ,  $-66^{\circ} 40'$  has on its outskirts N 63 and N 49 (the latter not listed in Table I due to its small size), believed to be supernova remnants (Westerlund and Mathewson 1966), also the HII region N 55 near low intensity HI only, and, in the south, the supergiant OB stars of the so-called Constellation III,  $05^{\text{h}} 28^{\text{m}}$ ,  $-67^{\circ} 28'$  (Nail and Shapley 1953).

A second hole in the HI may be seen in Figure 6(*b*) near  $05^{\text{h}} 28^{\text{m}}$ ,  $-69^{\circ}$ ; it corresponds in position with the supergiants of Constellation II,  $05^{\text{h}} 27^{\text{m}}$ ,  $-68^{\circ} 52'$ .

### (*b*) Population II

The term Population II is used here in a broad sense to include objects not covered under "Population I" above. The objects to be discussed apparently belong to either the "Bar" or the "Disk" subsystems defined by Westerlund (1965). The HI, HII, and extreme Population I stars form a "flat Central System" in Westerlund's table. Only a few comparisons are available both on radial velocity and positional data.





### 2.2. Young Populous Clusters

Fifteen of 28 observed by Hodge (1961) are near HI complexes. The numbers in 2.1 and 2.2 would indicate only chance agreement.

### 2.3. Clusters in the LMC

Two catalogues of clusters have been published. Lyngå and Westerlund (1963) surveyed the outer parts to find 483 clusters, and the search by Shapley and Lindsay (1963) resulted in 898 clusters over the whole Cloud area.

We have studied the latter by plotting the cluster positions and drawing contours of the distribution, as numbers per sq degree, in Figure 8. The dotted

TABLE 3  
PLANETARY NEBULAE AND NEUTRAL HYDROGEN IN THE LARGE MAGELLANIC CLOUD

Henize Number	Position		Radial Velocity (km/sec)	Radial Velocity at HI Profile Peak (km/sec)	Relative Intensity at HI Profile Peak	$\Delta$   (km/sec)
	R. A. h m	Dec. ° ' "				
N 184	04 48.5	-72 30	+274	+250	> 3	24
N 39	05 20.9	-67 09	+339	+314	20	25
N 42	05 21.6	-67 03	+300	+312	16	12
N 52	05 28.8	-67 36	+311	+302	12	9
N 153	05 34.7	-69 00	+235	—	0	—
N 211	05 36.6	-73 54	+237	+260	4	23
N 203	05 25.8	-73 41	+187	+256	2	69
N 210	05 35.7	-74 18	+234	+264	3	30
N 221	06 19.5	-71 35	+264	—	0	—
N 44A	05 21.6	-67 54	+300	+300	37	0

outline represents HI limits. The outer contour of 5 per sq degree is approximately circular, of diameter about  $7\frac{1}{2}^\circ$ . The Bar region, relatively deficient in HI, is prominent in Figure 8, being outlined by the 20 contour with a  $2^\circ$  by  $1^\circ$  central section at the 25 level. However, other features show some correspondence with the HI distribution. A 20 contour, centred on  $05^h$ ,  $-69^\circ$ , is close to the two sets of HI complexes in that region. Two spurs of the 15 contour extend to the prominent L2 and L12 complexes of the “+300” gas. A feature in the 10 contour near  $05^h 55^m$ ,  $-68^\circ 30'$  corresponds to the intense HI spur in that vicinity. Finally, at a low level, the cluster distribution which falls off near declination  $-74^\circ$  increases again near  $05^h$ ,  $-74^\circ$ , not far from the slight increase in HI (see Fig. 5). Westerlund (1964) has also remarked on this.

### 2.4. The Stars of the LMC Bar

The distributions of HI in Figures 6(a) and 6(c) indicate that, in the directions of the optical Bar, neutral hydrogen occurs only where HII regions are to be found. It will be proposed in Section VII(b) that these are, in fact, part of an arm in front of the Bar. Thus, we believe that comparatively small quantities of HI are to be found in the stellar regions of the Bar (see Fig. 6(b)).

The comparisons made in this section would strongly support Westerlund's (1965) structure of the LMC. The stellar Bar is the outstanding optical subsystem characterized by Population II. The main Population I constituents, closely associated with one another in motions and positions, are in an annular region between radii

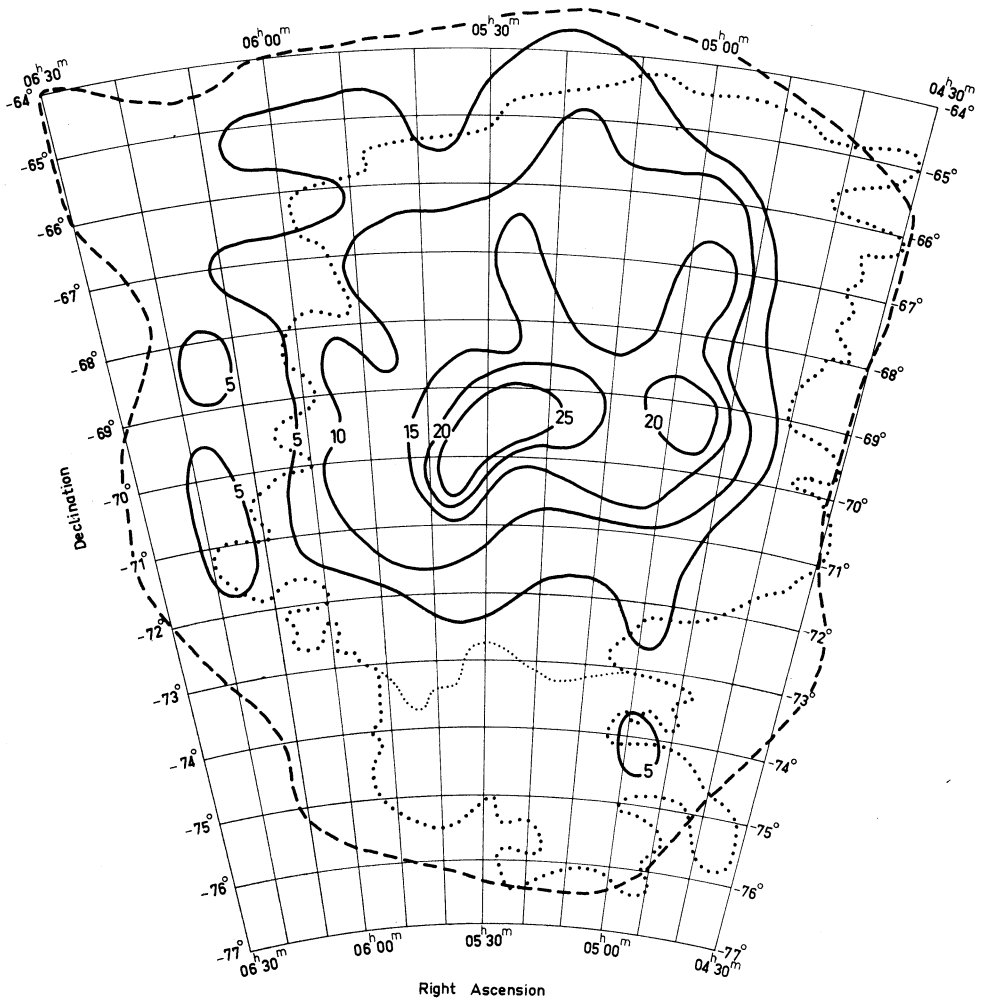


Fig. 8.—Contours of density of stellar clusters from the Shapley and Lindsay (1963) catalogue. The interval is 5 clusters per sq degree. . . . . outline of HI distribution.

of  $1^\circ$  and  $3^\circ$  approximately. Of greater dimensions ( $7\frac{1}{2}^\circ$  diam. at 5 per sq degree, and up to  $12\frac{1}{2}^\circ$  diam. as represented by the clusters of Fig. 8), but showing some relation with the latter, is the disk distribution of Population II. No grounds for comparison seem to exist for the spherical "halo" subsystem and the neutral gas. Finally, these indications agree with the findings of de Vaucouleurs (1960b) on the measurements of colour in the Cloud. When a mean colour index is plotted against radius,

it is found that the colour is bluer at  $2^{\circ}$ – $3^{\circ}$  radius than at the centre, while further out it rapidly becomes as red as the general sky background.

## VI. ROTATION OF THE LMC

In this section we examine the radial velocity data for the rotation of the LMC. We show that a unique rotation curve and inclination cannot be fitted to all the data. However, a curve of reasonable symmetry can be obtained using only the +300 and the +243 km/sec groups of velocities. Also, the shape of the intensity distribution of this gas leads us to an agreement with the inclination deduced from optical isophotes. It is proposed that the material characterized by these velocities represents two principal spiral arms of an SBc galaxy. The material characterized by the velocity +273 km/sec probably represents two secondary spiral arms inclined out of the principal plane and observed almost face on.

Whereas previous determinations of rotation curves have been based on some tens of values of radial velocity, the present survey has made available thousands of accurately measured profile peak velocities, should they be required.

### (a) *Previous Work*

The rotation of the Large Cloud has received extensive attention in the literature, particularly from Kerr and de Vaucouleurs (1955), de Vaucouleurs (1960a), Feast, Thackeray, and Wesselink (1961), and Feast (1964a).

The rotation of a galaxy can be detected only if the plane of rotation is inclined with respect to the line of sight. The usual method for establishing the inclination has been to study smoothed intensity contours and obtain a ratio of major to minor axes of the imagined ellipse. The assumption that the galaxy is a thin disk or ellipsoid is also required.

de Vaucouleurs (1957) used smoothed isophotes of red light and deduced that the major axis of the LMC was in position angle  $170^{\circ} \pm 5^{\circ}$  and that the angle between the line of sight and the normal to the equatorial plane,  $i$ , was  $27^{\circ}$ . Other values have been proposed: Lyngå and Westerlund (1963) found  $i = 45^{\circ}$ , Hindman, Kerr, and McGee (1963) gave  $i = 35^{\circ}$ . Feast, Thackeray, and Wesselink (1961) used the de Vaucouleurs value,  $i = 27^{\circ}$ , and were able to show that the variation in stellar velocities across the LMC is characterized by a vector  $813 \text{ km/sec} \pm 65 \text{ km/sec}$  in position angle  $171^{\circ} \pm 4^{\circ} \cdot 6$ .

### (b) *Fitting a Rotation Curve to the Radial Velocity Data*

A rotation centre and position angle for the major axis must first be selected before the data for a rotation curve can be assembled. Values of radial velocity were noted and distances from the rotation centre measured for points within sectors  $\pm 10^{\circ}$  from the position angle. The procedure was repeated for various centres and position angles until a satisfactory result was obtained.

The rotation curves were fitted with a digital computer program developed from methods described by Forsythe (1957) and Clenshaw (1960). A brief outline follows.

Let the distances of the points from the centre of rotation be  $r_0, r_1, \dots, r_n$ . A radial velocity  $V_0, V_1, \dots, V_n$  corresponds to each  $r$ . The rotation curve fitted to the  $n+1$  pairs of coordinates is a polynomial  $Y_k(r)$  of degree  $k$ , such that the residual sum of squares

$$\sum_{i=0}^n \{Y_k(r_i) - V_i\}^2 \quad (7)$$

is a minimum.  $Y_k(r)$  is obtained by truncating the series

$$C_0 p_0(r) + C_1 p_1(r) + C_2 p_2(r) + \dots \quad (8)$$

after  $k+1$  terms, where  $p_k(r)$  is a polynomial of degree  $k$  satisfying the orthogonality condition

$$\sum_i p_k(r_i) p_l(r_i) = 0 \quad (k \neq l). \quad (9)$$

Therefore, the coefficients  $C_i$  in (7) are

$$C_i = \frac{\sum_i V_i p_i(r_i)}{\sum_i \{p_i(r_i)\}^2}.$$

The  $p_k(r)$  may be computed successively from the recurrence formula

$$p_{k+1}(r) = \lambda_k(r - \alpha_{k+1}) p_k(r) - \beta_k p_{k-1}(r). \quad (10)$$

The generation of the polynomials by (10), and the computation of the coefficients  $C_i$  in

$$Y_k(r) = C_0 p_0(r) + C_1 p_1(r) + \dots + C_k p_k(r), \quad (11)$$

give the approximating polynomial of degree  $k$ . If  $k$  were allowed to take all values up to  $n$ , the approximating polynomial would pass through all  $n+1$  points  $(r_i, V_i)$ .

The polynomial of "best fit" is a compromise to obtain smoothness, as represented by the degree of the polynomial, and closeness to the data, as measured by equation (7). In practice, the best value of  $k$  is that for which the mean square of residuals, defined as

$$\sum_{i=0}^n \frac{\{Y_k(r_i) - V_i\}^2}{n-i},$$

ceases to decrease significantly.

Additional practical considerations concern the economy of storage in the computer and possible loss of accuracy with large coefficients, and so each polynomial in the computer is represented by the coefficients of its Chebyshev expansion. The details will not be further pursued here.

The observed velocities with respect to the Sun were corrected for a galactic rotation towards  $l^{\text{II}} = 90^\circ$ ,  $b^{\text{II}} = 0^\circ$  of values 216, 250, 270, and 300 km/sec. The corrections of 216, 270, and 300 km/sec enabled us to make direct comparisons with earlier rotation curves, but the 250 km/sec value, recommended by the IAU in 1963,\* has been used in all the curves presented below. The dashed contours in Figure 4 indicate how the corrections apply.

\* I.A.U. Information Bulletin No. 11 (1963). pp. 10-12.

*(c) A Rotation Curve from All Velocities*

The first curve (curve (i) of Figure 9) was obtained by fitting to points taken from the three velocity ranges. Its shape is similar to that of the original curve drawn by Kerr and de Vaucouleurs (1955), suitably replotted here as curve (ii). The same flattening is in evidence particularly in the negative, or southern, radius coordinates. Curve (ii) was based on observed profile median velocities which would have been reasonable averages of all the velocities we now detect individually.

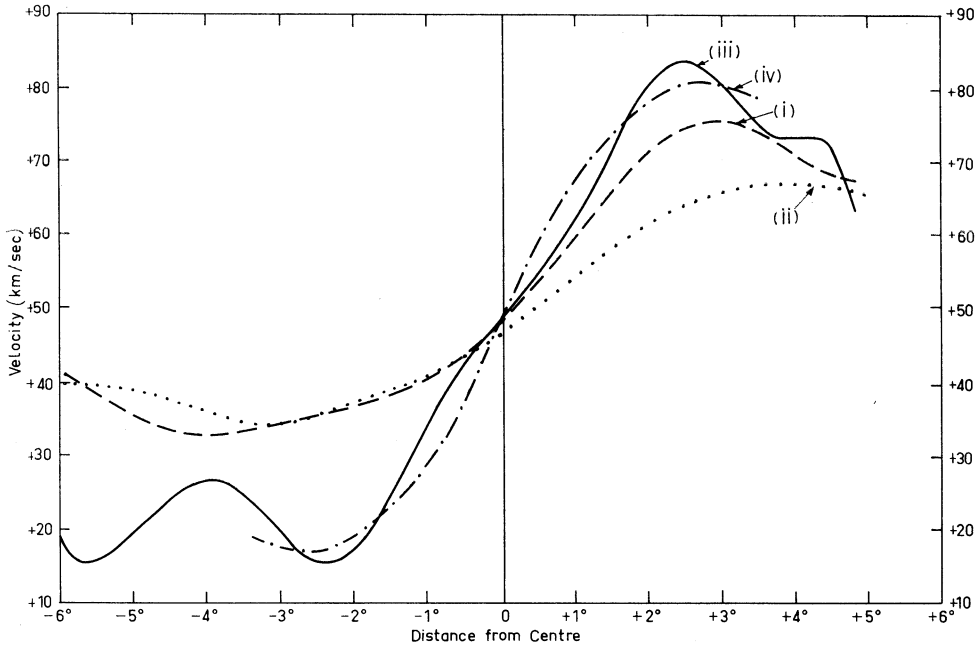


Fig. 9.—Rotation curves for the Large Magellanic Cloud. (i) Computer-fitted curve for all the points of Figure 10 of the present paper; (ii) curve taken from Figure 2 of Kerr and de Vaucouleurs (1955); (iii) curve A of Figure 10 of the present paper; (iv) curve taken from Figure 2 of Feast (1964a).

However, if the representative velocities of the HI complexes of Table 1 be regarded as carrying most weight and are compared with curve (i), we find that it is an unsatisfactory rotation curve. All the +300 group L1–L19, except one, have positive residuals; the mean is +7 km/sec with s.d.  $\pm 5.5$  km/sec. All the +243 group L34–L52 have negative residuals from curve (i); the mean is  $-13.5$  km/sec, s.d.  $\pm 6.5$  km/sec. Complexes L20–L33 are more widely scattered, the mean residual being  $-6.5$  km/sec, s.d.  $\pm 12.5$  km/sec. These relatively large residuals from what could be called the “average rotation curve” for the LMC support the idea of the existence of at least three separate large agglomerations of HI complexes.

Earlier radio observations led to the adoption of a centre of rotation, called the “radio centre”, at  $05^{\text{h}}20^{\text{m}}, -68^{\circ}.8$ . This point was defined by the condition that the resultant velocity curve would be symmetrical (Kerr and de Vaucouleurs

1956). Feast (1964*a*) found that the radio centre provided the best rotation curve for his Population I objects. Using the same symmetry criterion, we find the best centre of rotation is at  $05^{\text{h}}20^{\text{m}}$ ,  $-69^{\circ}0$  (see (*d*) below).

The centroid of the LMC, based on optical data, is at  $05^{\text{h}}24^{\text{m}}$ ,  $-69^{\circ}8$ . We have calculated a centroid for the 898 clusters discussed in Section V at  $05^{\text{h}}25^{\text{m}}$ ,  $-69^{\circ}8$ . According to Webster (1965), the most satisfactory centre of rotation for the only Population II objects for which data are available, namely, the planetary nebulae, is also close by, at  $05^{\text{h}}25^{\text{m}}$ ,  $-69^{\circ}5$ .

Thus, when we assume that the components of the LMC are describing circular orbits, we are faced with the apparent anomaly that the Population I objects, which form only a small fraction of the total mass, are rotating about a point of order 1 kpc from the centre of mass.

#### (*d*) Two Rotation Curves

Figure 10 shows 660 points from a  $20^{\circ}$  sector about position angle  $171^{\circ}$ , through a centre  $05^{\text{h}}20^{\text{m}}$ ,  $-69^{\circ}0$ . The three velocity groups are separately indicated (see legend). The differing character of the +273 points is immediately apparent; they are more widely scattered and extend over both the positive and the negative sides of the diagram.

In view of the dispositions of the +300 and +243 points in Figure 10 and the obvious counterbalancing nature of the gas at these velocities seen in Figure 5, a rotation curve, A, was fitted to them. The curve is almost symmetrical over a range  $\pm 3\frac{1}{2}^{\circ}$  from the centre. The first stationary points are at +35 km/sec,  $+2^{\circ}5$  and at -34 km/sec,  $-2^{\circ}4$  from the central values. A number of centres and position angles were tried before choosing  $05^{\text{h}}20^{\text{m}}$ ,  $-69^{\circ}0$  on the grounds of best symmetry. In particular, the optical centre,  $05^{\text{h}}24^{\text{m}}$ ,  $-69^{\circ}8$ , and the "radio centre",  $05^{\text{h}}20^{\text{m}}$ ,  $-68^{\circ}8$ , were tested. The value of position angle did not appear critical over  $\pm 15^{\circ}$ , but  $171^{\circ}$  was used on account of the findings of Feast, Thackeray, and Wesselink (1961).

The means of the residuals of the representative velocities of the +300 and +243 complexes from curve A are +1.5 km/sec, s.d.  $\pm 8$  km/sec and -0.5 km/sec, s.d.  $\pm 6.5$  km/sec respectively, indicating a great improvement.

Curve A is repeated in Figure 9 as curve (iii). It may be compared with Feast's (1964*a*) rotation curve derived from radial velocities of 42 HII nebulae and 61 supergiant stars. The average gradients out to the first stationary points are 14.6 and 14.2 km sec<sup>-1</sup> deg<sup>-1</sup> respectively. Both rotation curves are very close to the "adopted rotation curve" finally reached by Kerr and de Vaucouleurs (1956).

Curve B of Figure 10 was fitted to the +273 points. To obtain a "rotation" type curve, the "closeness" factor is much less than for A. The points from the +273 complexes, L20-L33, have a mean residual from curve B of only -1 km/sec, s.d.  $\pm 10.5$  km/sec. The gradient is 2.1 km sec<sup>-1</sup> deg<sup>-1</sup>. Trials of other centres of rotation for curve B suggested that the present one gives the closest approximation to symmetry.

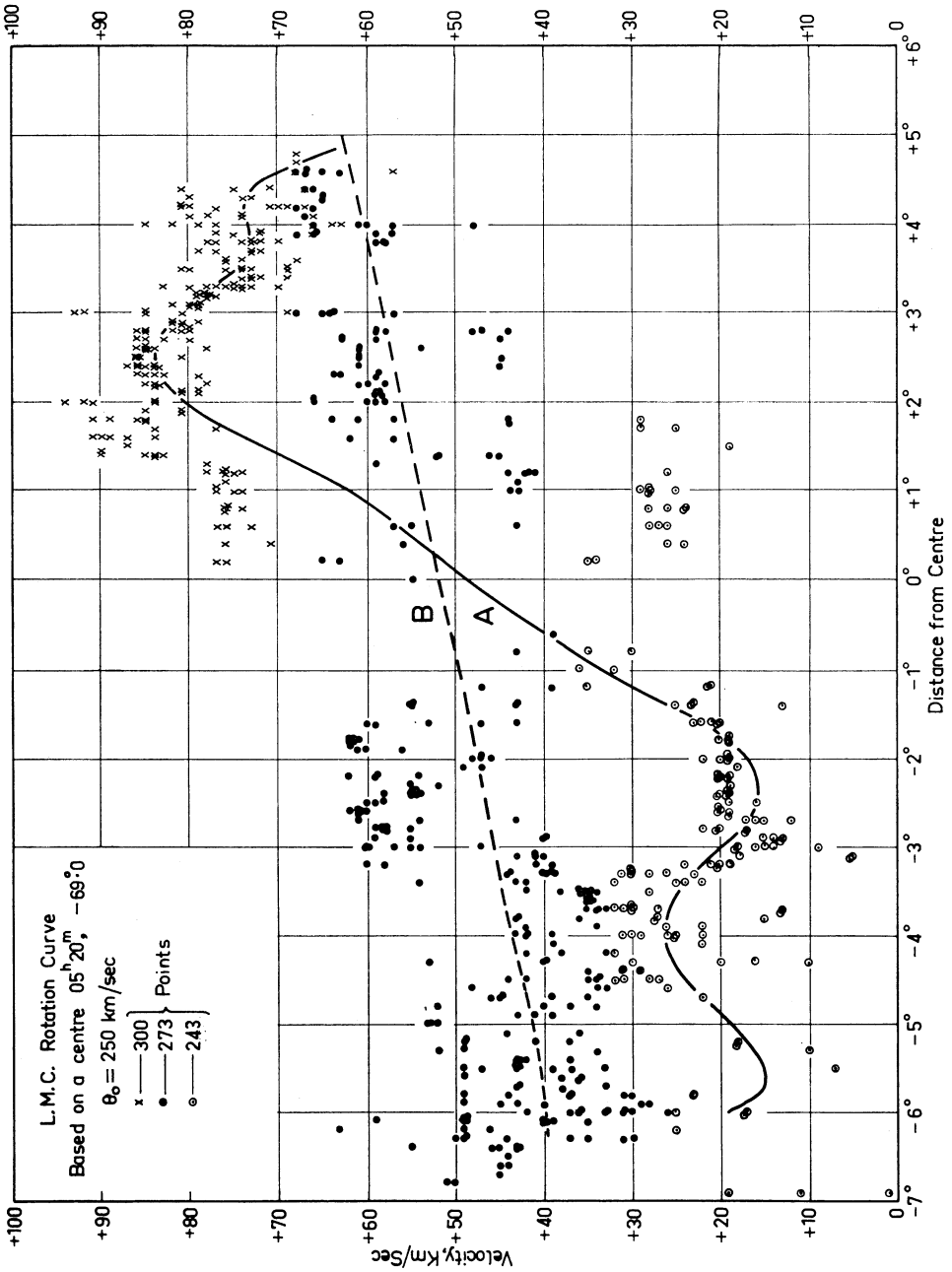


Fig. 10.—Data for the rotation curves. Coordinates are radial velocity and distance from the "centre". The points occur in a sector  $\pm 10^{\circ}$  from position angle  $171^{\circ}$ . Curve A has been fitted to the  $+300$  and  $+243$  points, curve B to the  $+273$  points.

*(e) Inclination*

The inclination  $i$  of the plane of rotation of the neutral hydrogen has been estimated in the usual way by fitting ellipses around the main body (i.e. between declinations  $-64^{\circ}30'$  and  $-73^{\circ}30'$ ) of the distribution in Figure 5. The results apply to the  $+300$  and  $+243$  gas. Values for  $i$  between  $23^{\circ}$  and  $32^{\circ}$  were found from several independent trials. Thus, in quoting  $i = 27^{\circ} \pm 5^{\circ}$  we have arrived at the most widely accepted value. We should emphasize that the method is inherently inaccurate and at  $i < 30^{\circ}$  is sensitive to small changes in the estimates of the ratio of axes.

A determination made on the diagram of the distribution of stellar clusters (Fig. 8) results in  $i = 25^{\circ} \pm 9^{\circ}$  in position angle  $171^{\circ}$ .

The irregular form of the  $+273$  distribution (see Fig. 6(b)) makes it impossible to estimate  $i_{273}$  in this way. If we assume that the LMC rotates as a cohesive whole, the difference in gradients of curves A and B suggests a difference in the inclinations of the respective gas masses such that

$$\frac{\operatorname{cosec} i_{273}}{\operatorname{cosec} i_{300,243}} = \frac{\text{gradient of curve A}}{\text{gradient of curve B}}$$

Taking  $i_{300,243}$  as  $27^{\circ}$ , we obtain  $i_{273} \approx 4^{\circ}$ .

In this way, we may reconcile the apparently asymmetrical rotation curve (Fig. 9(i)), based on all the data, with a simple model of two gas masses each with symmetrical rotation curves but differing inclinations. While this is not a unique solution, it is compatible with the not infrequently observed distributions in galaxies of the SBc type. NGC 925, seen in the Hubble Atlas of Galaxies (Sandage 1961), may be cited as an example where two large arms and at least one smaller arm at each end of its bar appear to be at different inclinations.

## VII. THE SPIRAL ARMS OF THE LMC

Plate 1 is a Mount Stromlo photograph of the Large Magellanic Cloud on which the outlines of the HI gas masses have been superimposed in white. Taken in conjunction with the Population I diagrams of Figure 7 and the rotation curve deductions of the previous section, this is convincing evidence of the spiral arm nature of the LMC. The two large bodies of gas at  $+300$  and  $+243$  km/sec belong to two spiral arms appearing from either end of the Bar; the two smaller bodies both at  $+273$  km/sec belong to two arms in a different plane. We now examine some aspects of these spiral components.

*(a) The Region Near 30 Doradus*

This region is important in the present context because it is the area where the  $+243$  arm starts and, presumably, separates from the south-going  $+273$  arm. The observed H-line profiles contain components of both velocity groups, but individual details are difficult to extract. Feast (1961) has measured radial velocities at 37 points in 30 Doradus, or the Tarantula Nebula, in some of the HII, and in some of the supergiant stars. Values extend from  $+234$  to  $+291$  km/sec. Although

Feast averaged the results to  $+260$  km/sec, the H-line profiles support the validity of all the measurements, as illustrated in Figure 11. In this figure, the optical velocities are shown by vertical lines, the lengths of which represent one, two, or three observations. The H-line profile for the direction  $05^{\text{h}} 39^{\text{m}} 09^{\text{s}}$ ,  $-69^{\circ} 06' \cdot 0$  is broad, with half-width  $48$  km/sec. Further observations made at bandwidth  $2$  km/sec failed to separate out individual components. The higher radio velocities have no optical counterparts.

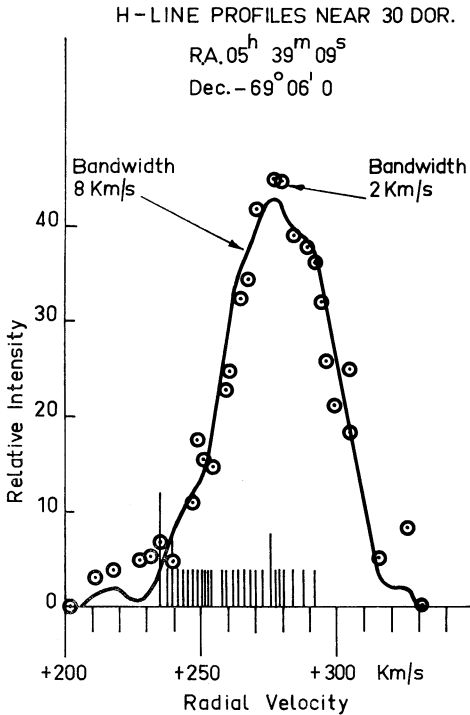


Fig. 11.—H-line profile near 30 Doradus. — observation with bandwidth  $\sim 8$  km/sec;  $\circ$  points measured with bandwidth  $2$  km/sec. The vertical lines indicate Feast's (1961) optical velocities.

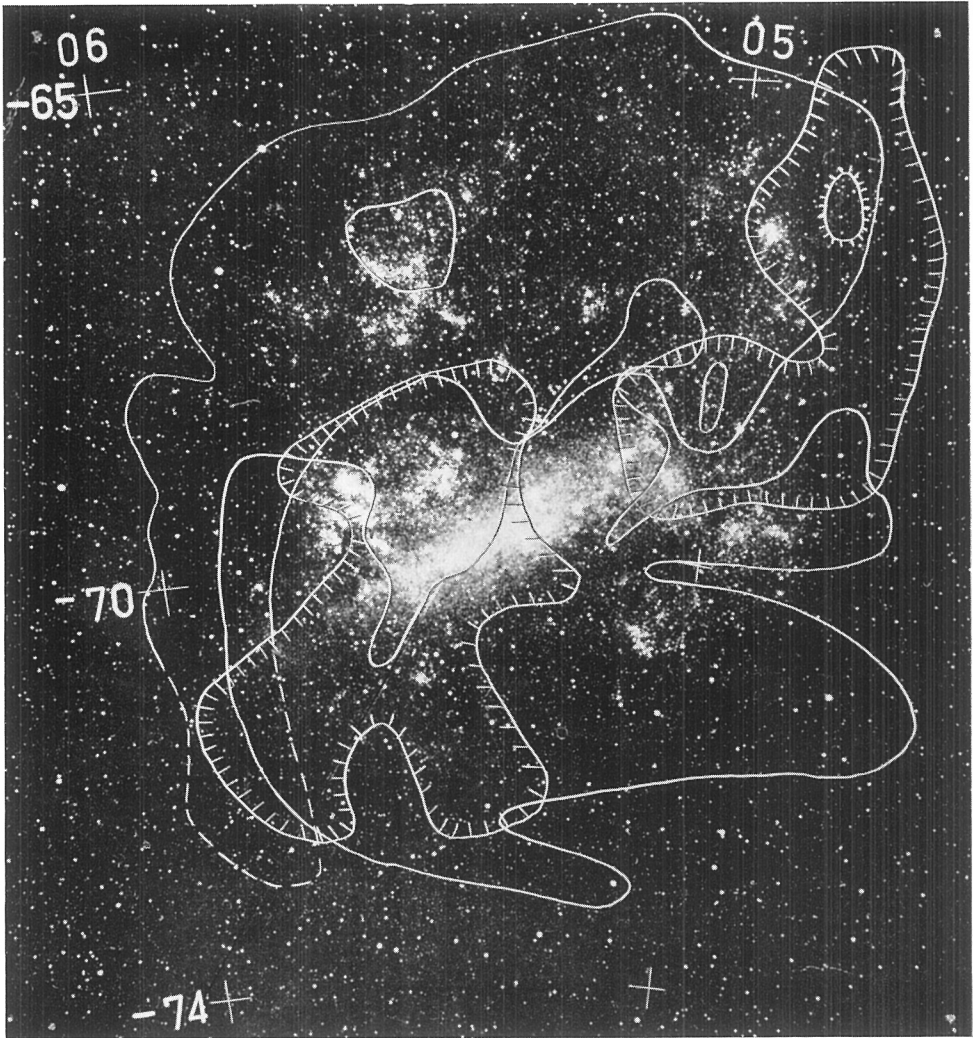
From the combined optical and radio data, it is inferred that both the  $+273$  and  $+243$  arms are associated with the nebula to some extent and that the  $+300$  arm in this direction must lie behind.

#### (b) The $+243$ Arm

The  $+243$  arm appears to the east and south of the Bar (Plate 1). HI is most strongly concentrated over the first  $2\frac{1}{2}$  kpc of its length. After a further  $1\frac{1}{2}$  kpc to the west, the arm divides into three large spurs whose widths are of the same order as the main body width of about  $2$  kpc.

The HI complexes L34–L52 contribute approximately half the mass of gas. Their close association with the other Population I components (see Fig. 7(c)) is strongly indicative of spiral arm phenomena.

## H-LINE SURVEY OF THE LARGE MAGELLANIC CLOUD. II



Neutral hydrogen spiral arms superimposed schematically on a Mount Stromlo photograph of the Large Magellanic Cloud. The full lines represent the +300 and +243 km/sec arms, the lines with hatching the two +273 km/sec arms.



In the area  $05^{\text{h}}35^{\text{m}}$  to  $05^{\text{h}}00^{\text{m}}$ ,  $-70^{\circ}30'$  to  $-72^{\circ}00'$ , the arm corresponds with a continuum feature of "an emissivity very similar to a galactic spiral arm" (Mathewson and Healey 1964).

The narrow neck of the north-going spur near  $05^{\text{h}}20^{\text{m}}$ ,  $-70^{\circ}30'$  corresponds exactly in position with the well-known lane of obscuration across the Bar. The spur contains many Population I objects and must lie in front of the stellar Bar.

(c) *The +300 Arm*

The beginning of the +300 arm (Plate 1) is not as marked as in the previous case. It is considered to be near  $04^{\text{h}}45^{\text{m}}$ ,  $-67^{\circ}$ , where a similar blending with +273 velocities occurs. The 19 HI complexes are more widely scattered in this arm and contribute only about one-third of its HI mass. The presence of other Population I objects in the arm and not elsewhere can again be noted in Figure 7(a).

The total length is estimated to be about 13 kpc, its average width about 2 kpc. The mass of HI,  $1.8 \times 10^8 M_{\odot}$ , is close to that of the +243 arm.

(d) *The +273 Arms*

Two arms are clearly distinguishable in Figures 6(b) and 7(b) as being of the same form and composition as those discussed in (b) and (c) above. The intensity contours show that some lower intensity gas may be associated with the Bar. An outward gradient in radial velocity of about  $5 \text{ km sec}^{-1} \text{ deg}^{-1}$  is observed in each direction along the Bar from  $05^{\text{h}}12^{\text{m}}$ ,  $-69^{\circ}$  approximately, which may mean that the gas is streaming outwards into each arm. The "hole" in the HI at  $05^{\text{h}}28^{\text{m}}$ ,  $-69^{\circ}30'$  is thought to be similar in character to that at  $05^{\text{h}}32^{\text{m}}$ ,  $-66^{\circ}50'$  in the +300 arm (Westerlund and Mathewson 1966).

### VIII. ESTIMATIONS OF TOTAL MASS AND MASS OF HI IN THE LMC

Perek (1962) has given a comprehensive treatment of the many methods used in the calculation of masses of galaxies, with particular application to some individual galaxies including the LMC. Despite the use of several methods, the best earlier estimates lie in a range of only 2 to 1. Thus we consider that only a simplified calculation is necessary here to show that the present data yield similar results.

A weakness in the determination is that the LMC is by no means a planar system, in view of the +273 arms and the +243 spur in front of the Bar (see Section VII(b)), so that in using the virial theorem as applied to a disk-like system we place merely a lower limit on the total mass.

The rotation curve A is used to supply data for the main contribution. We make an approximate calculation of an additional contribution due to random motions. Such motions are represented by a dispersion  $\sigma = 11.5 \text{ km/sec}$  (Table 2), a value close to the stellar dispersion  $10.5 \text{ km/sec}$  (Feast 1964a).

In the equation for mass

$$M = \frac{2V^2R}{G}(\text{rotational}) + \frac{2\bar{V}^2R}{G}(\text{random motions}), \quad (12)$$

we have

$$V = V^1 \operatorname{cosec} i \quad \text{at distance } R,$$

where, from curve A, Figure 10,

$$V^1 = (\text{observed velocity at } R = 2^\circ \cdot 45) - (\text{systemic velocity}) = 34 \text{ km/sec},$$

with

$$\operatorname{cosec} i = 2 \cdot 2,$$

$$R = 2 \cdot 22 \text{ kpc for LMC distance } 52 \text{ kpc},$$

$$G = \text{gravitational constant} = 6 \cdot 668 \text{ dyn cm}^2 \text{ gm}^{-2}.$$

Considering the gas system as a disk, we write

$$\begin{aligned} \bar{V}^2 &= \sigma^2(\text{line of sight}) + \sigma^2(\text{perpendicular to line of sight}) \\ &= 2\sigma^2 \quad \text{at an angular distance } R \text{ of } 4^\circ \cdot 2/\sqrt{2} \equiv 2 \cdot 72 \text{ kpc}. \end{aligned}$$

Then, from equation (12),

$$M \doteq (5 \cdot 8 \times 10^9 + 0 \cdot 3 \times 10^9) M_\odot = 6 \cdot 1 \times 10^9 M_\odot.$$

Feast (1964*a*) found that the mass of the LMC falls between  $0 \cdot 5 \times 10^{10} M_\odot$  and  $10^{10} M_\odot$ .

An estimate of the mass of neutral hydrogen was made directly from the data, by using equation (6) to obtain a relation for mass per sq parsec and integrating over the three  $T_{\max}$  contour diagrams of Figure 6. From (6),

$$\begin{aligned} \text{mass per sq parsec} &= 847 V_p M_\odot, \\ \text{mass of the } +300 \text{ gas} &= 1 \cdot 83 \times 10^8 M_\odot, \\ \text{mass of the } +273 \text{ gas} &= 1 \cdot 76 \times 10^8 M_\odot, \\ \text{mass of the } +243 \text{ gas} &= 1 \cdot 78 \times 10^8 M_\odot, \\ \text{total mass of HI in LMC} &= 5 \cdot 4 \times 10^8 M_\odot. \end{aligned}$$

Kerr, Hindman, and Robinson (1954) used integrated brightness contours to find a mass for HI of  $6 \times 10^8 M_\odot$ , a figure more recently verified by Hindman, Kerr, and McGee (1963).

It may be stated, then, that the ratio of mass of neutral hydrogen in the LMC to its total mass lies between 5 and 9%.

## IX. CONCLUSIONS

The analysis of the H-line observations has shed some new light on the structure of the Large Magellanic Cloud. The close association of the Population I constituents, HI, HII, and supergiant stars, established above, has produced a clear picture of its spiral arm nature. The LMC can scarcely be classified as an "irregular galaxy" in the face of this evidence.

The spiral arms themselves are seen to consist of enormous clouds of Population I objects. The average diameter of an HI complex is 580 pc, average mass  $4 \times 10^6 M_\odot$ , which places these objects in the largest class of neutral hydrogen cloud. The present aerial resolution, equivalent to 219 pc, prevented the discernment of any finer detail.

Estimates of the rotation of the galaxy, and the deductions from this concerning total mass, remain largely unchanged from the recent determinations. The modification in terms of two subsystems of spiral arms inclined at different angles is offered as a possible explanation of the distorted "rotation curve". However, the question of the rotation of the Population I objects about a centre removed from the centre of mass is still unanswered. It would seem that great advances could be made by obtaining information on the rotation of the Population II components. A start on this difficult task has already been made in the measurements of radial velocities of some planetary nebulae.

#### X. ACKNOWLEDGMENTS

We are grateful to Miss Diane Castleman and Mrs. Gillian Stumbles for the several digital computer programs and to Mr. H. C. K. Armstrong and Miss Heather Campbell for most helpful photographic assistance. The assistance of Mr. F. M. Carter of the Radiophysics Drawing Office and the preparation of the diagrams by Mrs. Margaret McBroom are appreciated. We acknowledge with pleasure the discussions and criticisms of Professor B. J. Bok, Mr. J. G. Bolton, Dr. B. J. Robinson, and Mr. J. V. Hindman.

#### XI. REFERENCES

- BOK, B. J. (1964).—*Scient. Am.* **210**: 32.  
 CLENSHAW, C. W. (1960).—*Comput. J.* **2**: 170–3.  
 FEAST, M. W. (1961).—*Mon. Not. R. Astr. Soc.* **122**: 1–16.  
 FEAST, M. W. (1964a).—*Mon. Not. R. Astr. Soc.* **127**: 195–214.  
 FEAST, M. W. (1964b).—*Observatory* **84**: 266–70.  
 FEAST, M. W., THACKERAY, A. D., and WESSELINK, A. J. (1960).—*Mon. Not. R. Astr. Soc.* **121**: 337–85.  
 FEAST, M. W., THACKERAY, A. D., and WESSELINK, A. J. (1961).—*Mon. Not. R. Astr. Soc.* **122**: 433–53.  
 FORSYTHE, G. E. (1957).—*J. Soc. Ind. Appl. Math.* **5**: 74–88.  
 GASCOIGNE, S. C. B., and KRON, G. E. (1965).—*Mon. Not. R. Astr. Soc.* **130**: 333–60.  
 HENZE, K. G. (1956).—*Astrophys. J. Suppl. Ser.* **2**: 315–44.  
 HINDMAN, J. V., KERR, F. J., and MCGEE, R. X. (1963).—*Aust. J. Phys.* **16**: 570–83.  
 HINDMAN, J. V., MCGEE, R. X., CARTER, A. W. L., HOLMES, E. L. J., and BEARD, M. (1963).—*Aust. J. Phys.* **16**: 552–69.  
 HODGE, P. W. (1960).—*Astrophys. J.* **131**: 351–3.  
 HODGE, P. W. (1961).—*Astrophys. J.* **133**: 413–19.  
 KERR, F. J., HINDMAN, J. V., and ROBINSON, B. J. (1954).—*Aust. J. Phys.* **7**: 297–314.  
 KERR, F. J., and RODGERS, A. W. (Eds.) (1964).—"The Galaxy and the Magellanic Clouds." (Proceedings of IAU-URSI Symposium No. 20 (Canberra 1963), published by the Australian Academy of Science.)  
 KERR, F. J., and DE VAUCOULEURS, G. (1955).—*Aust. J. Phys.* **8**: 508–22.  
 KERR, F. J., and DE VAUCOULEURS, G. (1956).—*Aust. J. Phys.* **9**: 90–111.  
 LYNGÅ, G., and WESTERLUND, B. E. (1963).—*Mon. Not. R. Astr. Soc.* **127**: 31–6.  
 MCGEE, R. X. (1964a).—*Aust. J. Phys.* **17**: 515–23.  
 MCGEE, R. X. (1964b).—Symp. IAU-URSI No. 20 (Canberra 1963). pp. 126–30.  
 MCGEE, R. X., and MILTON, JANICE A. (1964).—*Aust. J. Phys.* **17**: 128–57.  
 MCGEE, R. X., and MILTON, JANICE A. (1966).—*Aust. J. Phys. Astrophys. Suppl.* No. 2.  
 MCGEE, R. X., MILTON, JANICE A., and WOLFE, WENDY (1966).—*Aust. J. Phys. Astrophys. Suppl.* No. 1.

- MCGEE, R. X., and MURRAY, J. D. (1963).—*Proc. Instn Radio Engrs Aust.* **24**: 191-6.
- MCGEE, R. X., MURRAY, J. D., and MILTON, JANICE A. (1963).—*Aust. J. Phys.* **16**: 136-70.
- MATHEWSON, D. S., and HEALEY, J. R. (1964).—Symp. IAU-URSI No. 20 (Canberra 1963). pp. 245-55.
- NAIL, VIRGINIA MCK., and SHAPLEY, H. (1953).—*Proc. Natn. Acad. Sci. U.S.A.* **39**: 358-62.
- PEREK, L. (1962).—*Adv. Astr. & Astrophys.* **1**: 165-287.
- RAIMOND, E. (1966).—*Bull. Astr. Insts Neth. Suppl. Ser.* **1**, No. 2.
- SANDAGE, A. (1961).—"The Hubble Atlas of Galaxies." (Carnegie Institution of Washington.)
- SHAPLEY, H., and LINDSAY, M. (1963).—*Ir. Astr. J.* **6**: 74-91.
- THACKERAY, A. D. (1963).—*Adv. Astr. & Astrophys.* **2**: 263-304.
- DE VAUCOULEURS, G. (1957).—*Astr. J.* **62**: 69-82.
- DE VAUCOULEURS, G. (1960a).—*Astrophys. J.* **131**: 265-81.
- DE VAUCOULEURS, G. (1960b).—*Astrophys. J.* **131**: 574-84.
- WEBSTER, LOUISE (1965).—Mount Stromlo Symposium on the Magellanic Clouds, 1965. pp. 29-33. (Mount Stromlo Observatory: Canberra.)
- WESTERLUND, B. E. (1964).—*Observatory* **84**: 253-5.
- WESTERLUND, B. E. (1965).—Mount Stromlo Symposium on the Magellanic Clouds, 1965. pp. 40-5. (Mount Stromlo Observatory: Canberra.)
- WESTERLUND, B. E., and MATHEWSON, D. S. (1966).—*Mon. Not. R. Astr. Soc.* (in press).
- WILD, J. P. (1952).—*Astrophys. J.* **115**: 206-21.